Quantum theory of helimagnetic thin films

H. T. Diep*

Laboratoire de Physique Théorique et Modélisation, Université de Cergy-Pontoise, Centre National de la Recherche Scientifique, Unités Mixtes de Recherche, 8089 2 Avenue Adolphe Chauvin, 95302 Cergy-Pontoise Cedex, France

(Received 19 November 2014; revised manuscript received 9 January 2015; published 29 January 2015)

We study properties of a helimagnetic thin film with a quantum Heisenberg spin model by using the Green's-function method. Surface spin configuration is calculated by minimizing the spin interaction energy. It is shown that the angles between spins near the surface are strongly modified with respect to the bulk configuration. Taking into account this surface spin reconstruction, we calculate self-consistently the spin-wave spectrum and the layer magnetizations as functions of temperature up to the disordered phase. The spin-wave spectrum shows the existence of a surface-localized branch which causes a low surface magnetization. We show that quantum fluctuations give rise to a crossover between the surface magnetization and interior-layer magnetizations at low temperatures. We calculate the transition temperature and show that it depends strongly on the helical angle. Results are in agreement with existing experimental observations on the stability of helical structure in thin films and on the insensitivity of the transition temperature with the film thickness. We also study effects of various parameters such as surface exchange and anisotropy interactions. Monte Carlo simulations for the classical spin model are also carried out for comparison with the quantum theoretical result.

DOI: 10.1103/PhysRevB.91.014436 PACS number(s): 75.25.−j, 75.30.Ds, 75.70.−i

I. INTRODUCTION

Helimagnets have been discovered a long time ago by Yoshimori [1] and Villain [2]. In the simplest model, the helimagnetic ordering is noncollinear due to a competition between nearest-neighbor (NN) and next-nearest-neighbor (NNN) interactions: for example, a spin in a chain turns an angle θ with respect to its previous neighbor. Low-temperature properties in helimagnets such as spin waves [3–6] and heat capacity [7] have been extensively investigated. Helimagnets belong to a class of frustrated vector-spin systems. In spite of their long history, the nature of the phase transition in bulk helimagnets as well as in other noncollinear magnets such as stacked triangular XY and Heisenberg antiferromagnets has been elucidated only recently [8–10]. For reviews on many aspects of frustrated spin systems, the reader is referred to Ref. [11].

In this paper, we study a helimagnetic thin film with the quantum Heisenberg spin model. Surface effects in thin films have been widely studied theoretically, experimentally, and numerically, during the last three decades [12,13]. Nevertheless, surface effects in helimagnets have only been recently studied: surface spin structures [14], Monte Carlo (MC) simulations [15], magnetic field effects on the phase diagram in Ho [16], and a few experiments [17,18]. We will compare our work to these in the Conclusion.

Helical magnets present potential applications in spintronics with predictions of spin-dependent electron transport in these magnetic materials [19–21]. This has motivated the present work. We shall use the Green's-function (GF) method to study a quantum spin model on a helimagnetic thin film of a body-centered-cubic (bcc) lattice. The GF method has been initiated by Zubarev [22] for collinear bulk magnets (ferromagnets and antiferromagnets) and by Diep-The-Hung *et al.* for collinear surface spin configurations [23]. For noncollinear magnets, the GF method has also been developed for bulk helimagnets [6] and for frustrated films [24,25]. Note that surface effects in thin films of stacked triangular antiferromagnets with noncollinear 120° spin configuration have been investigated by the method of the equation of motion [26]. However, the model in these works did not possess a surface spin reconstruction and does not belong to the family of helical structures as our model described below.

In helimagnets, the presence of a surface modifies the competing forces acting on surface spins. As a consequence, as will be shown below, the angles between neighboring spins become nonuniform, making calculations harder. This explains why there is no microscopic calculation so far for helimagnetic films.

Note that for illustration we use below the bcc lattice structure, but the results obtained in this paper are valid for different lattices, not restricted to the bcc crystal, provided modifications on the coordination number and therefore on the value of the critical value $(J_2/J_1)_c$ (J_1, NNN interaction; J_2, NNN interaction). For example, the bcc case has $(J_2/J_1)_c = 1$ while the simple cubic lattice has $(J_2/J_1)_c = 1/4$.

The paper is organized as follows. In Sec. II, the model is presented and the classical ground state (GS) of the helimagnetic film is determined. In Sec. III, the general GF method for nonuniform spin configurations is shown in detail. The GF results are shown in Sec. IV where the spin-wave spectrum, the layer magnetizations, and the transition temperature are shown. Effects of surface interaction parameters and the film thickness are discussed. Concluding remarks are given in Sec. V.

II. MODEL AND CLASSICAL GROUND STATE

Let us recall that bulk helical structures are due to the competition of various kinds of interaction [1,2,27–29]. We consider hereafter the simplest model for a film: the helical ordering is along one direction, namely, the c axis perpendicular to the film surface.

*diep@u-cergy.fr

We consider a thin film of a bcc lattice of N_z layers, with two symmetrical surfaces perpendicular to the c axis, for simplicity. The exchange Hamiltonian reads

$$\mathcal{H} = \mathcal{H}_e + \mathcal{H}_a, \tag{1}$$

where the isotropic exchange part is given by

$$\mathcal{H}_e = -\sum_{\langle i,j\rangle} J_{i,j}\mathbf{S}_i \cdot \mathbf{S}_j, \tag{2}$$

$J_{i,j}$ being the interaction between two quantum Heisenberg spins $\mathbf{S}_i$ and $\mathbf{S}_j$ occupying the lattice sites i and j. The anisotropic part is chosen as

$$\mathcal{H}_a = -\sum_{\langle i,j\rangle} I_{i,j} S_i^z S_j^z \cos\theta_{ij}, \tag{3}$$

where $I_{i,j}$ is the anisotropic interaction along the in-plane local spin-quantization axes z of $\mathbf{S}_i$ and $\mathbf{S}_j$, supposed to be positive, small compared to J_1, and limited to NN on the c axis. Let us mention that according to the theorem of Mermin and Wagner [30] continuous isotropic spin models such as XY and Heisenberg spins do not have long-range ordering at finite temperatures in two dimensions. Since we are dealing with the Heisenberg model in a thin film, it is useful to add an anisotropic interaction to create a long-range ordering and a phase transition at finite temperatures.

To generate a bulk helimagnetic structure, the simplest way is to take a ferromagnetic interaction between NNs, say J_1 (>0), and an antiferromagnetic interaction between NNNs, $J_2 < 0$. It is obvious that if $|J_2|$ is smaller than a critical value $|J_2^c|$ the classical GS spin configuration is ferromagnetic [3–5]. Since our purpose is to investigate the helimagnetic structure near the surface and surface effects, let us consider the case of a helimagnetic structure only in the c direction perpendicular to the film surface. In such a case, we assume a nonzero J_2 only on the c axis. This assumption simplifies formulas but does not change the physics of the problem since including the uniform helical angles in two other directions parallel to the surface will not introduce additional surface effects. Note that the bulk case of the above quantum spin model has been studied by the Green's-function method [6].

Let us recall that the helical structure in the bulk is planar: spins lie in planes perpendicular to the c axis: the angle between two NNs in the adjacent planes is a constant and is given by $\cos\alpha = -J_1/J_2$ for a bcc lattice. The helical structure exists therefore if $|J_2| \geqslant J_1$, namely, $|J_2^c|$(bulk)$= J_1$ [see Fig. 1 (top)]. To simplify the presentation, we take a zero anisotropy $I_{i,j} = 0$. The effect of $I_{i,j}$ on the GS will be shown at the end of this section.

To calculate the classical GS surface spin configuration, we write down the expression of the energy of spins along the c axis, starting from the surface:

$$\begin{aligned} E = &-Z_1 J_1 \cos(\theta_1 - \theta_2) - Z_1 J_1[\cos(\theta_2 - \theta_1) + \cos(\theta_2 - \theta_3)] \\ &+ \ldots - J_2\cos(\theta_1 - \theta_3) - J_2\cos(\theta_2 - \theta_4) \\ &- J_2[\cos(\theta_3 - \theta_1) + \cos(\theta_3 - \theta_5)] + \ldots, \end{aligned} \tag{4}$$

where $Z_1 = 4$ is the number of NNs in a neighboring layer and θ_i denotes the angle of a spin in the ith layer made with the Cartesian x axis of the layer. The interaction energy between two NN spins in the two adjacent layers i and j depends only on the difference $\alpha_i \equiv \theta_i - \theta_{i+1}$. The GS configuration corresponds to the minimum of E. We have to solve the set of equations:

$$\frac{\partial E}{\partial \alpha_i} = 0, \quad \text{for} \quad i = 1, N_z - 1. \tag{5}$$

Explicitly, we have

$$\frac{\partial E}{\partial \alpha_1} = 8J_1 \sin\alpha_1 + 2J_2 \sin(\alpha_1 + \alpha_2) = 0, \tag{6}$$

$$\begin{aligned} \frac{\partial E}{\partial \alpha_2} = &\ 8J_1 \sin\alpha_2 + 2J_2 \sin(\alpha_1 + \alpha_2) \\ &+ 2J_2 \sin(\alpha_2 + \alpha_3) = 0, \end{aligned} \tag{7}$$

$$\begin{aligned} \frac{\partial E}{\partial \alpha_3} = &\ 8J_1 \sin\alpha_3 + 2J_2 \sin(\alpha_2 + \alpha_3) \\ &+ 2J_2 \sin(\alpha_3 + \alpha_4) = 0, \end{aligned} \tag{8}$$

$$\frac{\partial E}{\partial \alpha_4} = \ldots,$$

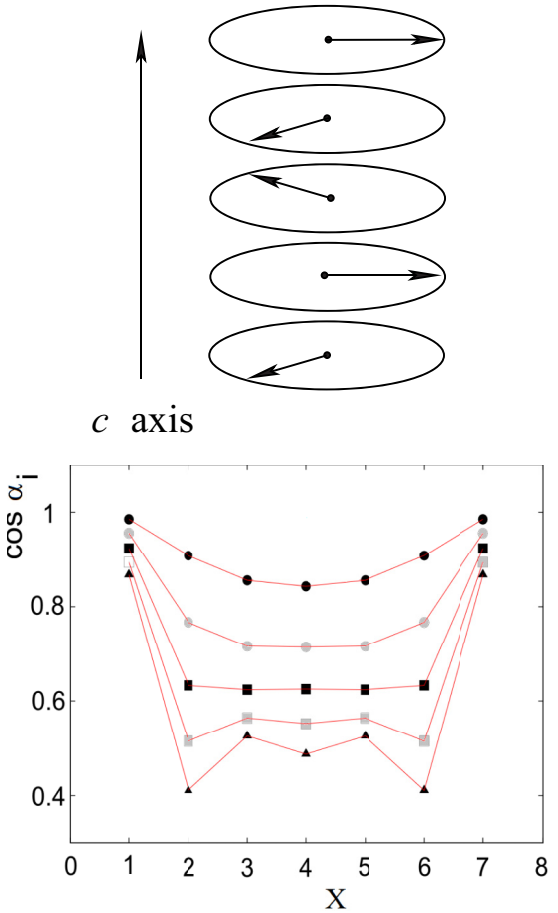

FIG. 1. (Color online) Top: Bulk helical structure along the c axis, in the case $\alpha = 2\pi/3$, namely, $J_2/J_1 = -2$. Bottom: Cosinus of $\alpha_1 = \theta_1 - \theta_2, \ldots, \alpha_7 = \theta_7 - \theta_8$ across the film for $J_2/J_1 = -1.2, -1.4, -1.6, -1.8, -2$ (from top) with $N_z = 8$; a_i stands for $\theta_i - \theta_{i+1}$ and x indicates the film layer i where the angle a_i with the layer $(i+1)$ is shown. The values of the angles are given in Table I: a strong rearrangement of spins near the surface is observed.

TABLE I. Values of $\cos\theta_{n,n+1} = \alpha_n$ between two adjacent layers are shown for various values of J_2/J_1. Only angles of the first half of the eight-layer film are shown: other angles are, by symmetry, $\cos\theta_{7,8}$=$\cos\theta_{1,2}$, $\cos\theta_{6,7}$=$\cos\theta_{2,3}$, $\cos\theta_{5,6}$=$\cos\theta_{3,4}$. The values in parentheses are angles in degrees. The last column shows the value of the angle in the bulk case (infinite thickness). For presentation, angles are shown with two digits.

J_2/J_1	$\cos\theta_{1,2}$	$\cos\theta_{2,3}$	$\cos\theta_{3,4}$	$\cos\theta_{4,5}$	α(bulk)
−1.2	0.985(9.79°)	0.908(24.73°)	0.855(31.15°)	0.843(32.54°)	33.56°
−1.4	0.955(17.07°)	0.767(39.92°)	0.716(44.28°)	0.714(44.41°)	44.42°
−1.6	0.924(22.52°)	0.633(50.73°)	0.624(51.38°)	0.625(51.30°)	51.32°
−1.8	0.894(26.66°)	0.514(59.04°)	0.564(55.66°)	0.552(56.48°)	56.25°
−2.0	0.867(29.84°)	0.411(65.76°)	0.525(58.31°)	0.487(60.85°)	60°

where we have expressed the angle between two NNNs as follows: $\theta_1 - \theta_3 = \theta_1 - \theta_2 + \theta_2 - \theta_3 = \alpha_1 + \alpha_2$, etc. In the bulk case, putting all angles α_i in Eq. (7) equal to α we get $\cos\alpha = -J_1/J_2$ as expected. For the spin configuration near the surface, let us consider in the first step only three parameters: α_1 (between the surface and the second layer), α_2, and α_3. We take $\alpha_n = \alpha$ from $n = 4$ inward up to $n = N_z/2$, the other half being symmetric. Solving the first two equations, we obtain

$$\tan\alpha_2 = -\frac{2J_2(\sin\alpha_3 + \sin\alpha_1)}{8J_1 + 2J_2(\cos\alpha_3 + \cos\alpha_1)}. \tag{9}$$

The iterative numerical procedure is as follows: (1) replacing α_3 by $\alpha = \arccos(-J_1/J_2)$ and solving Eqs. (6) and (9) to obtain α_1 and α_2, (2) replacing these values into Eq. (8) to calculate α_3, (3) using this value of α_3 to solve again Eqs. (6) and (9) to obtain new values of α_1 and α_2, and (4) repeating steps 2 and 3 until the convergence is reached within a desired precision. In the second step, we use α_1, α_2, and α_3 to calculate by iteration α_4, assuming a bulk value for α_5. In the third step, we use α_i ($i = 1 - 4$) to calculate α_5, and so on. The results calculated for various J_2/J_1 are shown in Fig. 1 (bottom) for a film of $N_z = 8$ layers. The values obtained are shown in Table I. Results of $N_z = 16$ will be shown later.

Some remarks are in order.

(i) The result shown is obtained by iteration with errors less than 10^{-4} degrees.

(ii) Strong angle variations are observed near the surface with oscillation for strong J_2.

(iii) The angles at the film center are close to the bulk value α (last column), meaning that the surface reconstruction affects just a few atomic layers.

(iv) The bulk helical order is stable just a few atomic layers away from the surface even for films thicker than $N_z = 8$ (see below). This helical stability has been experimentally observed in holmium films [31].

Note that using the numerical steepest descent method described in Ref. [24] we find the same result.

Let us discuss now the effect of the anisotropy on the GS configuration. The form of Eq. (3) simplifies a lot: since the interaction is limited to NN, it suffices to replace in Eq. (4) the parameter J_1 by $J_1' = J_1 + I_1$, where $I_1 = I_{i,j}$ for any NN pairs (i,j). The GS calculation is done exactly in the same manner. That is the reason why we choose the form of Eq. (3). The GS configuration is slightly modified but the method and the general aspects of the results described above remain valid. Of course, the calculations of the spin-wave spectrum and layer magnetizations presented below take into account the GS modification at each value of I_1. Choosing another form of anisotropy, for example, taking a standard single-ion anisotropy $-I(S_i^z)^2$ along the spin local axis, will add just a constant in Eq. (4) [because $(S_i^z)^2 = 1$ in the GS]. So, it will not affect the GS configuration. This is not our interest.

In the following, using the spin configuration obtained at each J_2/J_1 we calculate the spin-wave excitation and properties of the film such as the zero-point spin contraction, the layer magnetizations, and the critical temperature.

III. GREEN'S-FUNCTION METHOD

Let us define the local spin coordinates as follows: the quantization axis of spin $\vec{S}_i$ is on its ζ_i axis which lies in the plane, the η_i axis of $\vec{S}_i$ is along the c axis, and the ξ_i axis forms with η_i and ζ_i axes a direct trihedron. Since the spin configuration is planar, all spins have the same η axis. Furthermore, all spins in a given layer are parallel. Let $\hat{\xi}_i$, $\hat{\eta}_i$, and $\hat{\zeta}_i$ be the unit vectors on the local (ξ_i,η_i,ζ_i) axes. We use the following local transformation which has been used for the first time in Ref. [3] and described in Ref. [33]:

$$\vec{S}_i = S_i^x\hat{\xi}_i + S_i^y\hat{\eta}_i + S_i^z\hat{\zeta}_i, \tag{10}$$

$$\vec{S}_j = S_j^x\hat{\xi}_j + S_j^y\hat{\eta}_j + S_j^z\hat{\zeta}_j. \tag{11}$$

We have (see Fig. 2)

$$\begin{aligned}\hat{\xi}_j &= \cos\theta_{ij}\hat{\zeta}_i + \sin\theta_{ij}\hat{\xi}_i,\\ \hat{\zeta}_j &= -\sin\theta_{ij}\hat{\zeta}_i + \cos\theta_{ij}\hat{\xi}_i,\\ \hat{\eta}_j &= \hat{\eta}_i,\end{aligned}$$

where $\cos\theta_{ij} = \cos(\theta_i - \theta_j)$ is the angle between two spins i and j.

Note that in the laboratory coordinate system, namely, in the film coordinates, the z direction coincides with the c direction or the $\hat{\eta}$ axis perpendicular to the film surface, while the x and y directions are taken to be the bcc crystal axes in the film plane.

Replacing these into Eq. (11) to express $\vec{S}_j$ in the $(\hat{\xi}_i,\hat{\eta}_i,\hat{\zeta}_i)$ coordinates, then calculating $\vec{S}_i \cdot \vec{S}_j$, we obtain the following

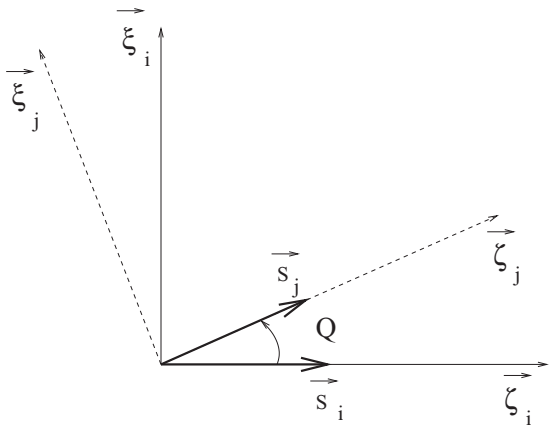

FIG. 2. Local coordinates in a xy plane perpendicular to the c axis. Q denotes $\theta_j - \theta_i$.

exchange Hamiltonian from Eq. (2):

$$\mathcal{H}_e = -\sum_{\langle i,j\rangle} J_{i,j}\Big\{\frac{1}{4}(\cos\theta_{ij}-1)(S_i^+S_j^+ + S_i^-S_j^-) + \frac{1}{4}(\cos\theta_{ij}+1)(S_i^+S_j^- + S_i^-S_j^+) + \frac{1}{2}\sin\theta_{ij}(S_i^+ + S_i^-)S_j^z - \frac{1}{2}\sin\theta_{ij}S_i^z(S_j^+ + S_j^-) + \cos\theta_{ij}S_i^zS_j^z\Big\}. \quad (12)$$

A. General formulation for noncollinear magnets

We define the following two double-time Green's functions in the real space:

$$G_{i,j}(t,t') = \langle\langle S_i^+(t); S_j^-(t')\rangle\rangle = -i\theta(t-t')\langle[S_i^+(t), S_j^-(t')]\rangle, \quad (13)$$

$$F_{i,j}(t,t') = \langle\langle S_i^-(t); S_j^-(t')\rangle\rangle = -i\theta(t-t')\langle[S_i^-(t), S_j^-(t')]\rangle. \quad (14)$$

We need these two functions because the equation of motion of the first function generates functions of the second type, and vice versa. These equations of motion are

$$i\hbar\frac{d}{dt}G_{i,j}(t,t') = \langle[S_i^+(t), S_j^-(t')]\rangle\delta(t-t') - \langle\langle[\mathcal{H}, S_i^+(t)]; S_j^-(t')\rangle\rangle, \quad (15)$$

$$i\hbar\frac{d}{dt}F_{i,j}(t,t') = \langle[S_i^-(t), S_j^-(t')]\rangle\delta(t-t') - \langle\langle[\mathcal{H}, S_i^-(t)]; S_j^-(t')\rangle\rangle, \quad (16)$$

where the spin operators and their commutation relations are given by

$$S_j^\pm = S_j^x\hat{\xi}_j \pm iS_j^y\hat{\eta}_j,$$
$$[S_j^+, S_l^-] = 2S_j^z\delta_{j,l},$$
$$[S_j^z, S_l^\pm] = \pm S_j^\pm\delta_{j,l}.$$

Expanding the commutators in Eqs. (15) and (16), and using the Tyablikov decoupling scheme [32] for higher-order functions, for example, $\langle\langle S_{i'}^zS_i^+(t); S_j^-(t')\rangle\rangle \simeq \langle S_{i'}^z\rangle\langle\langle S_i^+(t); S_j^-(t')\rangle\rangle$, etc., we obtain the following general equations for noncollinear magnets:

$$i\hbar\frac{dG_{i,j}(t,t')}{dt} = 2\langle S_i^z\rangle\delta_{i,j}\delta(t-t') - \sum_{i'}J_{i,i'}\big[\langle S_i^z\rangle(\cos\theta_{i,i'}-1)F_{i',j}(t,t') + \langle S_i^z\rangle(\cos\theta_{i,i'}+1)G_{i',j}(t,t') - 2\langle S_{i'}^z\rangle\cos\theta_{i,i'}G_{i,j}(t,t')\big] + 2\sum_{i'}I_{i,i'}\langle S_{i'}^z\rangle\cos\theta_{i,i'}G_{i,j}(t,t'), \quad (17)$$

$$i\hbar\frac{dF_{i,j}(t,t')}{dt} = \sum_{i'}J_{i,i'}\big[\langle S_i^z\rangle(\cos\theta_{i,i'}-1)G_{i',j}(t,t') + \langle S_i^z\rangle(\cos\theta_{i,i'}+1)F_{i',j}(t,t') - 2\langle S_{i'}^z\rangle\cos\theta_{i,i'}F_{i,j}(t,t')\big] - 2\sum_{i'}I_{i,i'}\langle S_{i'}^z\rangle\cos\theta_{i,i'}F_{i,j}(t,t'). \quad (18)$$

B. Body-centered-cubic helimagnetic films

In the case of a bcc thin film with a (001) surface, the above equations yield a closed system of coupled equations within the Tyablikov decoupling scheme [32]. For clarity, we separate the sums on NN interactions and NNN interactions as follows:

$$i\hbar\frac{dG_{i,j}(t,t')}{dt} = 2\langle S_i^z\rangle\delta_{i,j}\delta(t-t') - \sum_{k'\in\mathrm{NN}}J_{i,k'}\big[\langle S_i^z\rangle(\cos\theta_{i,k'}-1)F_{k',j}(t,t') + \langle S_i^z\rangle(\cos\theta_{i,k'}+1)G_{k',j}(t,t') - 2\langle S_{k'}^z\rangle\cos\theta_{i,k'}G_{i,j}(t,t')\big] + 2\sum_{k'\in\mathrm{NN}}I_{i,k'}\langle S_{k'}^z\rangle\cos\theta_{i,k'}G_{i,j}(t,t') - \sum_{i'\in\mathrm{NNN}}J_{i,i'} \times\big[\langle S_i^z\rangle(\cos\theta_{i,i'}-1)F_{i',j}(t,t') + \langle S_i^z\rangle(\cos\theta_{i,i'}+1) \times G_{i',j}(t,t') - 2\langle S_{i'}^z\rangle\cos\theta_{i,i'}G_{i,j}(t,t')\big], \quad (19)$$

$$i\hbar\frac{dF_{k,j}(t,t')}{dt} = \sum_{i'\in\mathrm{NN}}J_{k,i'}\big[\langle S_k^z\rangle(\cos\theta_{k,i'}-1)G_{i',j}(t,t') + \langle S_k^z\rangle(\cos\theta_{k,i'}+1)F_{i',j}(t,t') - 2\langle S_{i'}^z\rangle\cos\theta_{k,i'}F_{k,j}(t,t')\big] - 2\sum_{i'\in\mathrm{NN}}I_{k,i'}\langle S_{i'}^z\rangle\cos\theta_{k,i'}F_{k,j}(t,t') + \sum_{k'\in\mathrm{NNN}}J_{k,k'} \times\big[\langle S_k^z\rangle(\cos\theta_{k,k'}-1)G_{k',j}(t,t') + \langle S_k^z\rangle(\cos\theta_{k,k'}+1) \times F_{k',j}(t,t') - 2\langle S_{k'}^z\rangle\cos\theta_{k,k'}F_{k,j}(t,t')\big]. \quad (20)$$

For simplicity, except otherwise stated, all NN interactions $(J_{k,k'}, I_{k,k'})$ are taken equal to (J_1, I_1) and all NNN interactions are taken equal to J_2 in the following. Furthermore, let us denote, in the film coordinates defined above, the Cartesian components of the spin position $\mathbf{R}_i$ by (ℓ_i, m_i, n_i).

We now introduce the following in-plane Fourier transforms:

$$G_{i,j}(t,t') = \frac{1}{\Delta}\int\int_{\mathrm{BZ}} d\mathbf{k}_{xy}\frac{1}{2\pi}\int_{-\infty}^{+\infty} d\omega e^{-i\omega(t-t')} \times g_{n_i,n_j}(\omega,\mathbf{k}_{xy})e^{i\mathbf{k}_{xy}\cdot(\mathbf{R}_i-\mathbf{R}_j)}, \quad (21)$$

$$F_{k,j}(t,t') = \frac{1}{\Delta}\int\int_{\mathrm{BZ}} d\mathbf{k}_{xy}\frac{1}{2\pi}\int_{-\infty}^{+\infty} d\omega e^{-i\omega(t-t')} \times f_{n_k,n_j}(\omega,\mathbf{k}_{xy})e^{i\mathbf{k}_{xy}\cdot(\mathbf{R}_k-\mathbf{R}_j)}, \quad (22)$$

where ω is the spin-wave frequency, $\mathbf{k}_{xy}$ denotes the wave vector parallel to xy planes, and $\mathbf{R}_i$ is the position of the spin at the site i. n_i, n_j, and n_k are, respectively, the z-component indices of the layers to which the sites $\mathbf{R}_i$, $\mathbf{R}_j$, and $\mathbf{R}_k$ belong. The integral over $\mathbf{k}_{xy}$ is performed in the first Brillouin zone (BZ) whose surface is Δ in the xy reciprocal plane. For convenience, we denote $n_i = 1$ for all sites on the surface layer, $n_i = 2$ for all sites of the second layer, and so on.

Note that, for a three-dimensional (3D) case, making a 3D Fourier transformation of Eqs. (19) and (20) we obtain the spin-wave dispersion relation in the absence of anisotropy:

$$\hbar\omega = \pm\sqrt{A^2 - B^2}, \quad (23)$$

where

$$A = J_1\langle S^z\rangle[\cos\theta + 1]Z\gamma + 2ZJ_1\langle S^z\rangle\cos\theta + J_2\langle S^z\rangle[\cos(2\theta) + 1]Z_c\cos(k_z a) + 2Z_cJ_2\langle S^z\rangle\cos(2\theta),$$

$$B = J_1\langle S^z\rangle(\cos\theta - 1)Z\gamma + J_2\langle S^z\rangle[\cos(2\theta) - 1]Z_c\cos(k_z a),$$

where $Z = 8$ (NN number), $Z_c = 2$ (NNN number on the c axis), and $\gamma = \cos(k_x a/2)\cos(k_y a/2)\cos(k_z a/2)$ (a: lattice constant). We see that $\hbar\omega$ is zero when $A = \pm B$, namely, at $k_x = k_y = k_z = 0$ ($\gamma = 1$) and at $k_z = 2\theta$ along the helical axis. The case of ferromagnets (antiferromagnets) with NN interaction only is recovered by putting $\cos\theta = 1$ (-1) [23].

Let us return to the film case. We make the in-plane Fourier transformation Eqs. (21) and (22) for Eqs. (19) and (20). We obtain the following matrix equation:

$$\mathbf{M}(\omega)\,\mathbf{h} = \mathbf{u}, \quad (24)$$

where $\mathbf{M}(\omega)$ is a square matrix of dimension $(2N_z \times 2N_z)$ and $\mathbf{h}$ and $\mathbf{u}$ are the column matrices which are defined as follows:

$$\mathbf{h} = \begin{pmatrix} g_{1,n'} \\ f_{1,n'} \\ \vdots \\ g_{n,n'} \\ f_{n,n'} \\ \vdots \\ g_{N_z,n'} \\ f_{N_z,n'} \end{pmatrix}, \quad \mathbf{u} = \begin{pmatrix} 2\langle S_1^z\rangle\delta_{1,n'} \\ 0 \\ \vdots \\ 2\langle S_{N_z}^z\rangle\delta_{N_z,n'} \\ 0 \end{pmatrix}, \quad (25)$$

where, taking $\hbar = 1$ hereafter,

$$\mathbf{M}(\omega) = \begin{pmatrix} \omega + A_1 & 0 & B_1^+ & C_1^+ & D_1^+ & E_1^+ & 0 & 0 & 0 & 0 & 0 & 0 \\ 0 & \omega - A_1 & -C_1^+ & -B_1^+ & -E_1^+ & -D_1^+ & 0 & 0 & 0 & 0 & 0 & 0 \\ \cdots & \cdots & \cdots & \cdots & \cdots & \cdots & \cdots & \cdots & \cdots & \cdots & \cdots & \cdots \\ \cdots & D_n^- & E_n^- & B_n^- & C_n^- & \omega + A_n & 0 & B_n^+ & C_n^+ & D_n^+ & E_n^+ & \cdots \\ \cdots & -E_n^- & -D_n^- & -C_n^- & -B_n^- & 0 & \omega - A_n & -C_n^+ & -B_n^+ & -E_n^+ & -D_n^+ & \cdots \\ \cdots & \cdots & \cdots & \cdots & \cdots & \cdots & \cdots & \cdots & \cdots & \cdots & \cdots & \cdots \\ 0 & 0 & 0 & 0 & 0 & 0 & D_{N_z}^- & E_{N_z}^- & B_{N_z}^- & C_{N_z}^- & \omega + A_{N_z} & 0 \\ 0 & 0 & 0 & 0 & 0 & 0 & -E_{N_z}^- & -D_{N_z}^- & -C_{N_z}^- & -B_{N_z}^- & 0 & \omega - A_{N_z} \end{pmatrix}, \quad (26)$$

where

$$A_n = -8J_1(1+d)\left[\langle S_{n+1}^z\rangle\cos\theta_{n,n+1} + \langle S_{n-1}^z\rangle\cos\theta_{n,n-1}\right] - 2J_2\left[\langle S_{n+2}^z\rangle\cos\theta_{n,n+2} + \langle S_{n-2}^z\rangle\cos\theta_{n,n-2}\right],$$

where $n = 1,2,\ldots,N_z$, $d = I_1/J_1$, and

$$B_n^{\pm} = 4J_1\langle S_n^z\rangle(\cos\theta_{n,n\pm1} + 1)\gamma,$$
$$C_n^{\pm} = 4J_1\langle S_n^z\rangle(\cos\theta_{n,n\pm1} - 1)\gamma,$$
$$E_n^{\pm} = J_2\langle S_n^z\rangle(\cos\theta_{n,n\pm2} - 1),$$
$$D_n^{\pm} = J_2\langle S_n^z\rangle(\cos\theta_{n,n\pm2} + 1).$$

In the above expressions, $\theta_{n,n\pm1}$ is the angle between a spin in the layer n and its NN spins in layers $n \pm 1$, etc., and $\gamma = \cos(\frac{k_x a}{2})\cos(\frac{k_y a}{2})$.

Solving $\det|\mathbf{M}| = 0$, we obtain the spin-wave spectrum ω of the present system: for each value (k_x, k_y), there are $2N_z$ eigenvalues of ω corresponding to two opposite spin precessions as in antiferromagnets (the dimension of $\det|\mathbf{M}|$ is $2N_z \times 2N_z$). Note that the above equation depends on the values of $\langle S_n^z\rangle$ ($n = 1,\ldots,N_z$). Even at temperature $T = 0$, these z components are not equal to $1/2$ because we are dealing with an antiferromagnetic system where fluctuations at $T = 0$ give rise to the so-called zero-point

spin contraction [33]. Worse, in our system with the existence of the film surfaces, the spin contractions are not spatially uniform as will be seen below. So the solution of $\det|\mathbf{M}| = 0$ should be found by iteration. This will be explicitly shown hereafter.

The solution for $g_{n,n}$ is given by

$$g_{n,n}(\omega) = \frac{|\mathbf{M}|_{2n-1}}{|\mathbf{M}|}, \tag{27}$$

where $|\mathbf{M}|_{2n-1}$ is the determinant made by replacing the $2n-1$th column of $|\mathbf{M}|$ by $\mathbf{u}$ given by Eq. (25) [note that $g_{n,n}$ occupies the $(2n-1)$th line of the matrix $\mathbf{h}$]. Writing now

$$|\mathbf{M}| = \prod_i [\omega - \omega_i(\mathbf{k}_{xy})], \tag{28}$$

we see that $\omega_i\left(\mathbf{k}_{xy}\right), i = 1,\ldots,2N_z$ are poles of $g_{n,n}$. $\omega_i\left(\mathbf{k}_{xy}\right)$ can be obtained by solving $|\mathbf{M}| = 0$. In this case, $g_{n,n}$ can be expressed as

$$g_{n,n}(\omega) = \sum_i \frac{D_{2n-1}[\omega_i(\mathbf{k}_{xy})]}{[\omega - \omega_i(\mathbf{k}_{xy})]}, \tag{29}$$

where $D_{2n-1}[\omega_i(\mathbf{k}_{xy})]$ is

$$D_{2n-1}[\omega_i(\mathbf{k}_{xy})] = \frac{|\mathbf{M}|_{2n-1}\,[\omega_i(\mathbf{k}_{xy})]}{\prod_{j\neq i}[\omega_j(\mathbf{k}_{xy}) - \omega_i(\mathbf{k}_{xy})]}. \tag{30}$$

Next, using the spectral theorem which relates the correlation function $\langle S_i^- S_j^+\rangle$ to the Green's function [22], we have

$$\langle S_i^- S_j^+\rangle = \lim_{\varepsilon\to 0}\frac{1}{\Delta}\int\int d\mathbf{k}_{xy}\int_{-\infty}^{+\infty}\frac{i}{2\pi}[g_{n,n'}(\omega + i\varepsilon) - g_{n,n'}(\omega - i\varepsilon)]\frac{d\omega}{e^{\beta\omega}-1}e^{i\mathbf{k}_{xy}\cdot(\mathbf{R}_i-\mathbf{R}_j)}, \tag{31}$$

where ϵ is an infinitesimal positive constant and $\beta = (k_B T)^{-1}$, k_B being the Boltzmann constant.

Using the Green's function presented above, we can calculate self-consistently various physical quantities as functions of temperature T. The magnetization $\langle S_n^z\rangle$ of the nth layer is given by

$$\begin{aligned}\langle S_n^z\rangle &= \frac{1}{2} - \langle S_n^- S_n^+\rangle \\ &= \frac{1}{2} - \lim_{\epsilon\to 0}\frac{1}{\Delta}\int\int d\mathbf{k}_{\mathbf{xy}}\int_{-\infty}^{+\infty}\frac{i}{2\pi}[g_{n,n}(\omega + i\epsilon) - g_{n,n}(\omega - i\epsilon)]\frac{d\omega}{e^{\beta\omega}-1}.\end{aligned} \tag{32}$$

Replacing Eq. (29) in Eq. (32) and making use of the following identity,

$$\frac{1}{x - i\eta} - \frac{1}{x + i\eta} = 2\pi i\delta(x), \tag{33}$$

we obtain

$$\langle S_n^z\rangle = \frac{1}{2} - \frac{1}{\Delta}\int\int dk_x dk_y \sum_{i=1}^{2N_z}\frac{D_{2n-1}(\omega_i)}{e^{\beta\omega_i}-1}, \tag{34}$$

where $n = 1,\ldots,N_z$. As $\langle S_n^z\rangle$ depends on the magnetizations of the neighboring layers via $\omega_i (i = 1,\ldots,2N_z)$, we should solve by iteration Eq. (34) written for all layers, namely, for $n = 1,\ldots,N_z$, to obtain the magnetizations of layers $1,2,3,\ldots,N_z$ at a given temperature T. Note that by symmetry $\langle S_1^z\rangle = \langle S_{N_z}^z\rangle$, $\langle S_2^z\rangle = \langle S_{N_z-1}^z\rangle$, $\langle S_3^z\rangle = \langle S_{N_z-2}^z\rangle$, and so on. Thus, only $N_z/2$ self-consistent layer magnetizations are to be calculated.

The value of the spin in the layer n at $T = 0$ is calculated by

$$\langle S_n^z\rangle(T=0) = \frac{1}{2} + \frac{1}{\Delta}\int\int dk_x dk_y \sum_{i=1}^{N_z} D_{2n-1}(\omega_i), \tag{35}$$

where the sum is performed over N_z negative values of ω_i (for positive values the Bose-Einstein factor is equal to zero at $T = 0$).

The transition temperature T_c can be calculated in a self-consistent manner by iteration, letting all $\langle S_n^z\rangle$ tend to zero, namely, $\omega_i \to 0$. Expanding $e^{\beta\omega_i} - 1 \to \beta_c\omega_i$ on the right-hand side of Eq. (34) where $\beta_c = (k_B T_c)^{-1}$, we have, by putting $\langle S_n^z\rangle = 0$ on the left-hand side,

$$\beta_c = 2\frac{1}{\Delta}\int\int dk_x dk_y \sum_{i=1}^{2N_z}\frac{D_{2n-1}(\omega_i)}{\omega_i}. \tag{36}$$

There are N_z such equations using Eq. (34) with $n = 1,\ldots,N_z$. Since the layer magnetizations tend to zero at the transition temperature from different values, it is obvious that we have to look for a convergence of the solutions of Eq. (36) to a single value of T_c. The method to do this will be shown below.

IV. RESULTS FROM THE GREEN'S-FUNCTION METHOD

Let us take $J_1 = 1$, namely, ferromagnetic interaction between NN. We consider the helimagnetic case where the NNN interaction J_2 is negative and $|J_2| > J_1$. The nonuniform GS spin configuration across the film has been determined in Sec. II for each value of $p = J_2/J_1$. Using the values of $\theta_{n,n\pm1}$ and $\theta_{n,n\pm2}$ to calculate the matrix elements of $|\mathbf{M}|$, then solving $\det|\mathbf{M}| = 0$, we find the eigenvalues $\omega_i (i = 1,\ldots,2N_z)$ for each $\mathbf{k}_{xy}$ with an input set of $\langle S_n^z\rangle (n = 1,\ldots,N_z)$ at a given T. Using Eq. (34) for $n = 1,\ldots,N_z$ we calculate the output $\langle S_n^z\rangle (n = 1,\ldots,N_z)$. Using this output set as input, we calculate again $\langle S_n^z\rangle (n = 1,\ldots,N_z)$ until the input and output are identical within a desired precision P. Numerically, we use a Brillouin zone of 100^2 wave-vector values, and we use the obtained values $\langle S_n^z\rangle$ at a given T as input for a neighboring T. At low T and up to $\sim\frac{4}{5}T_c$, only a few iterations suffice to get $P \leqslant 1\%$. Near T_c, several dozen iterations are needed to get convergence. We show below our results.

A. Spectrum

We calculated the spin-wave spectrum as described above for each given J_2/J_1. The spin-wave spectrum depends on the temperature via the temperature dependence of layer magnetizations. Let us show in Fig. 3 the spin-wave frequency ω versus $k_x = k_y$ in the case of an eight-layer film where

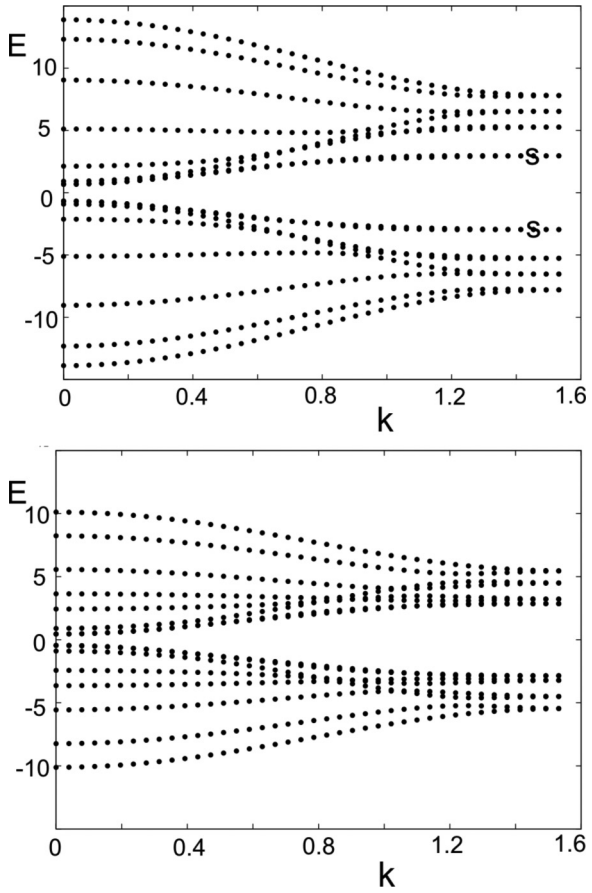

FIG. 3. Spectrum $E = \hbar\omega$ vs $k \equiv k_x = k_y$ for $J_2/J_1 = -1.4$ at $T = 0.1$ (top) and $T = 1.02$ (bottom) for $N_z = 8$ and $d = 0.1$. The surface branches are indicated by s.

$J_2/J_1 = -1.4$ at two temperatures $T = 0.1$ and 1.02 (in units of $J_1/k_B = 1$). Some remarks are in order:

(i) There are eight positive and eight negative modes corresponding to two opposite spin precessions. Unlike ferromagnets, spin waves in antiferromagnets and noncollinear spin structures have opposite spin precessions which describe the opposite circular motion of each sublattice spins [33]. The negative sign does not mean spin-wave negative energy, but it indicates just the precession contrary to the trigonometric sense.

(ii) Note that there are two degenerate acoustic surface branches lying at low energy on each side. This degeneracy comes from the two symmetrical surfaces of the film. These surface modes propagate parallel to the film surface but are damped from the surface inward.

(iii) As T increases, layer magnetizations decrease (see below), reducing therefore the spin-wave energy as seen in Fig. 3 (bottom).

(iv) If the spin magnitude $S \neq 1/2$, then the spectrum is shifted toward higher frequency since it is proportional to S.

(v) The surface spin-wave spectrum (and bulk spin waves) can be experimentally observed by inelastic neutron scattering in ferromagnetic and antiferromagnetic films [12,13]. To our knowledge, such experiments have not been performed for helimagnets.

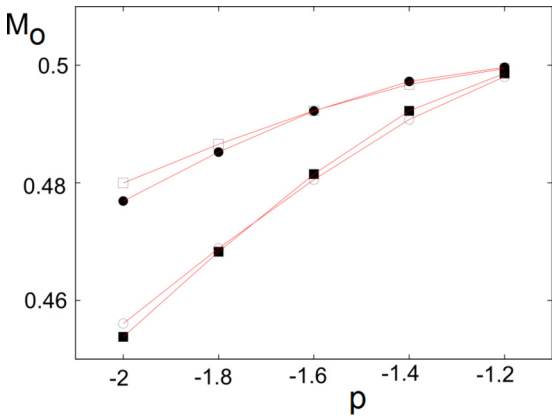

FIG. 4. (Color online) Spin lengths of the first four layers at $T = 0$ for several values of $p = J_2/J_1$ with $d = 0.1$, $N_z = 8$. Black circles, void circles, black squares, and void squares are for first, second, third, and fourth layers, respectively. See text for comments.

B. Spin contraction at $T = 0$ and transition temperature

It is known that in antiferromagnets quantum fluctuations give rise to a contraction of the spin length at zero temperature [33]. We will see here that a spin under a stronger antiferromagnetic interaction has a stronger zero-point spin contraction. The spins near the surface serve for such a test. In the case of the film considered above, spins in the first and in the second layers have only one antiferromagnetic NNN while interior spins have two NNNs, so the contraction at a given J_2/J_1 is expected to be stronger for interior spins. This is verified with the results shown in Fig. 4. When $|J_2|/J_1$ increases, namely, the antiferromagnetic interaction becomes stronger, we observe stronger contractions. Note that the contraction tends to zero when the spin configuration becomes ferromagnetic, namely, J_2 tends to -1.

C. Layer magnetizations

Let us show two examples of the magnetization, layer by layer, from the film surface in Figs. 5 and 6, for the case where $J_2/J_1 = -1.4$ and -2 in a $N_z = 8$ film. Let us comment on the case $J_2/J_1 = -1.4$.

(i) The shown result is obtained with a convergence of 1%. For temperatures closer to the transition temperature T_c, we have to lower the precision to a few percent which reduces the clarity because of their close values (not shown).

(ii) The surface magnetization, which has a large value at $T = 0$ as seen in Fig. 4, crosses the interior layer magnetizations at $T \simeq 0.42$ to become much smaller than interior magnetizations at higher temperatures. This crossover phenomenon is due to the competition between quantum fluctuations, which dominate low-T behavior, and the low-lying surface spin-wave modes which strongly diminish the surface magnetization at higher T. Note that the second-layer magnetization makes also a crossover at $T \simeq 1.3$. Similar crossovers have been observed in quantum antiferromagnetic films [34] and quantum superlattices [35].

Similar remarks can be also made for the case $J_2/J_1 = -2$.

Note that though the layer magnetizations are different at low temperatures they will tend to zero at a unique transition

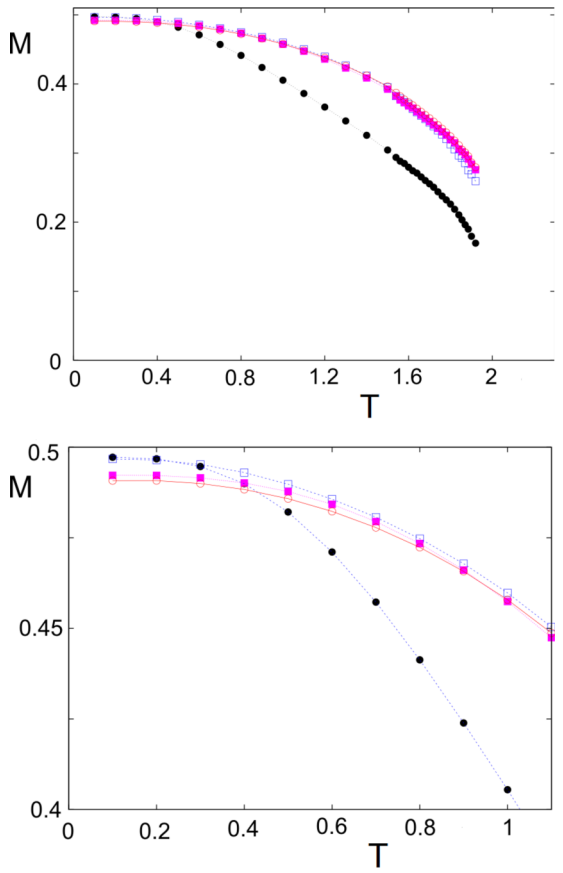

FIG. 5. (Color online) Layer magnetizations as functions of T for $J_2/J_1 = -1.4$ with $d = 0.1$, $N_z = 8$ (top). Zoom of the region at low T to show crossover (bottom). Black circles, blue void squares, magenta squares, and red void circles are for first, second, third, and fourth layers, respectively. See text.

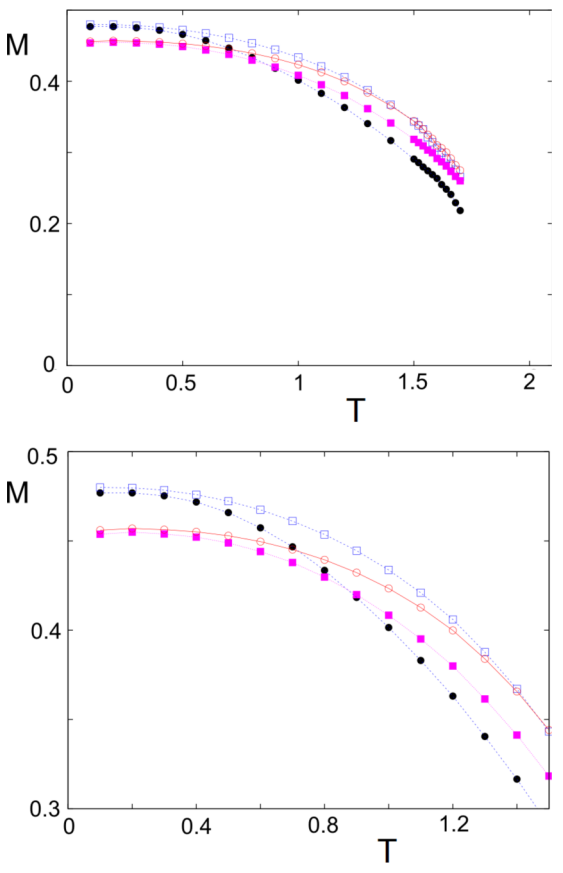

FIG. 6. (Color online) Layer magnetizations as functions of T for $J_2/J_1 = -2$ with $d = 0.1$, $N_z = 8$ (top). Zoom of the region at low T to show crossover (bottom). Black circles, blue void squares, magenta squares, and red void circles are for first, second, third, and fourth layers, respectively. See text.

temperature as seen below. The reason is that as long as an interior layer magnetization is not zero it will act on the surface spins as an external field, preventing them from becoming zero.

The temperature where layer magnetizations tend to zero is calculated by Eq. (36). Since all layer magnetizations tend to zero from different values, we have to solve self-consistently N_z Eq. (36) to obtain the transition temperature T_c. One way to do it is to use the self-consistent layer magnetizations obtained as described above at a temperature as close as possible to T_c as input for Eq. (36). As long as the T is far from T_c the convergence is not reached: we have four "pseudotransition temperatures" T_{cs} as seen in Fig. 7, one for each layer. The convergence of these T_{cs} can be obtained by a short extrapolation from temperatures when they are rather close to each other. T_c is thus obtained with a very small extrapolation error as seen in Fig. 7 for $p = J_2/J_1 = -1.4$: $T_c \simeq 2.313 \pm 0.010$. The results for several $p = J_2/J_1$ are shown in Fig. 8.

D. Effect of anisotropy and surface parameters

The results shown above have been calculated with an in-plane anisotropy interaction $d = 0.1$. Let us show now the effect of d. Stronger d will enhance all the layer magnetizations and increase T_c. Figure 9 shows the surface magnetization versus T for several values of d (other layer magnetizations are not shown to preserve the figure clarity). The transition temperatures are 2.091 ± 0.010, 2.313 ± 0.010, 2.752 ± 0.010, 3.195 ± 0.010, and 3.630 ± 0.010 for $d = 0.05, 0.1, 0.2, 0.3$, and 0.4, respectively. These values versus d lie on a remarkably straight line.

Let us examine the effects of the surface anisotropy and exchange parameters d_s and J_1^s. As seen above, even in the case where the surface interaction parameters are the same as those in the bulk the surface spin-wave modes exist in the spectrum. These localized modes cause a low surface magnetization, observed in Figs. 5 and 6. Here, we show that with a weaker NN exchange interaction between surface spins and the second-layer ones, namely, $J_1^s < J_1$, the surface magnetization becomes much smaller with respect to the magnetizations of interior layers. This is shown in Fig. 10 for several values of J_1^s. We observe again here the crossover of layer magnetizations at low T due to quantum fluctuations as discussed earlier. The transition temperature strongly decreases with J_1^s: we have $T_c = 2.103 \pm 0.010$, 1.951 ± 0.010, 1.880 ± 0.010, and 1.841 ± 0.010 for $J_1^s = 1, 0.7, 0.5$, and 0.3, respectively ($N_z = 16$, $J_2/J_1 = -2$, $d = d_s = 0.1$). Note that the value $J_1^s = 0.5$ is a very particular value: the GS configuration is a uniform

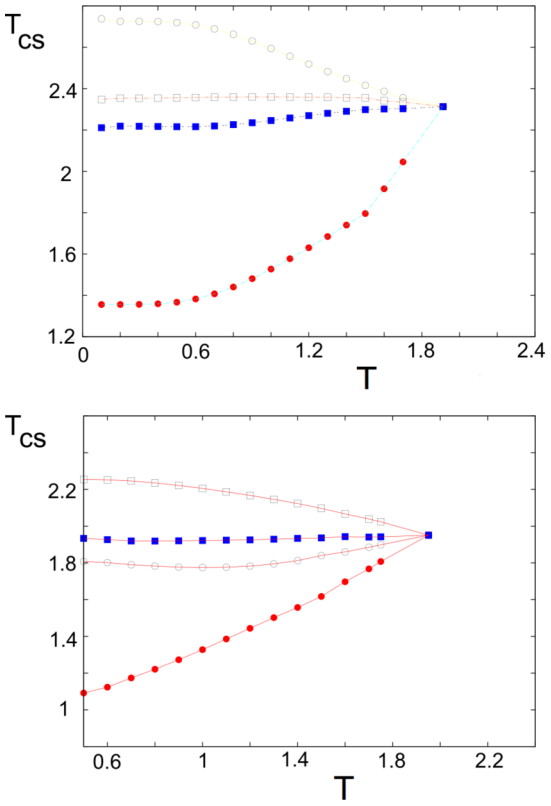

FIG. 7. (Color online) Top: Transition temperature is calculated at $p = J_2/J_1 = -1.4$ for $d = 0.1$, $N_z = 8$; at each temperature, using the self-consistent values of layer magnetizations at $T < T_c$, Eq. (36) is solved to obtain T_{cs} for each layer. The convergence is reached when T_{cs} tend to a single value T_c. One has $T_c \simeq 2.313 \pm 0.010$. Red circles, black void circles, blue squares, and blue void squares are T_{cs} obtained from Eq. (36) for first, second, third, and fourth layers, respectively, at different temperatures. Bottom: Extrapolation by lines to obtain T_c is shown for surface parameter $J_1^s/J_1 = 0.7$. The precision for self-consistent convergence is 1% for layer magnetizations. See text for comments.

configuration with all angles equal to 60°; namely, there is no surface spin rearrangement. This can be explained if we look at the local field acting on the surface spins: the lack of neighbors

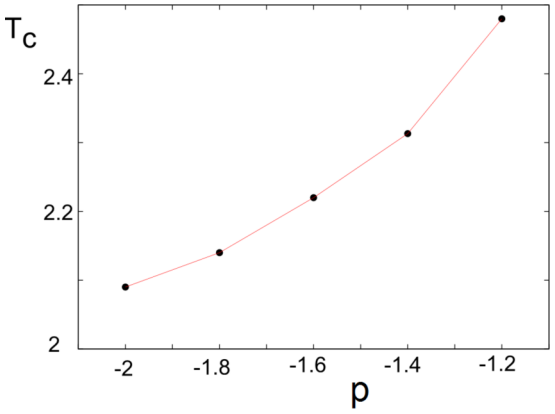

FIG. 8. (Color online) Transition temperature vs $p = J_2/J_1$ for an eight-layer film with $d = 0.1$. See text for comments.

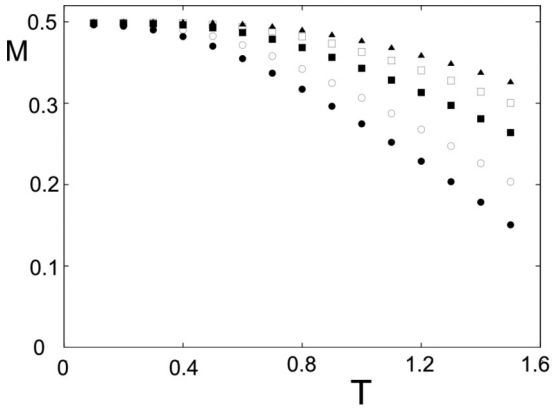

FIG. 9. Surface magnetization vs T for $d = 0.05$ (circles), 0.1 (void circles), 0.2 (squares), 0.3 (void squares), and 0.4 (triangles), with $J_2/J_1 = -1.4$, $N_z = 16$.

is compensated by this weak positive value of J_1^s so that their local field is equal to that of a bulk spin. There is thus no surface reconstruction. Nevertheless, as T increases, thermal effects will strongly diminish the surface magnetization as seen in Fig. 10 (middle). As for the surface anisotropy parameter d_s, it affects strongly the layer magnetizations and the transition temperature: we show in Fig. 11 the surface magnetizations and the transition temperature for several values of d_s.

E. Effect of the film thickness

We have performed calculations for $N_z = 8$, 12, and 16. The results show that the effect of the thickness at these values is not significant: the difference lies within convergence errors. Note that the classical ground states of the first four layers are almost the same: for example, here are the values of the cosinus of the angles of the first half of the film for $N_z = 16$, which are to be compared with the values for $N_z = 8$ given in Table I, for $p = J_2/J_1 = -2$ (in parentheses are angles in degree): 0.86737967 (29.844446), 0.41125694 (65.716179), 0.52374715 (58.416061), 0.49363765 (60.420044), 0.50170541 (59.887100), 0.49954081 (60.030373), 0.50013113 (59.991325), 0.49993441 (60.004330).

From the fourth layer, the angle is almost equal to the bulk value (60°).

At $p = J_2/J_1 = -2$, the transition temperature is 2.090 ± 0.010 for $N_z = 8$, 2.093 ± 0.010 for $N_z = 12$, and 2.103 ± 0.010 for $N_z = 16$. These are the same within errors. At smaller thicknesses, the difference can be seen. However, for helimagnets in the z direction, thicknesses smaller than 8 do not allow us to see fully the surface helical reconstruction which covers the first four layers: to study surface helical effects in such a situation would not make sense.

At this stage, it is interesting to note that our result is in excellent agreement with experiments: it has been experimentally observed that the transition temperature does not vary significantly in MnSi films in the thickness range of 11–40 nm [17]. One possible explanation is that the helical structure is very stable as seen above: the surface perturbs the bulk helical configuration only at the first four layers, so

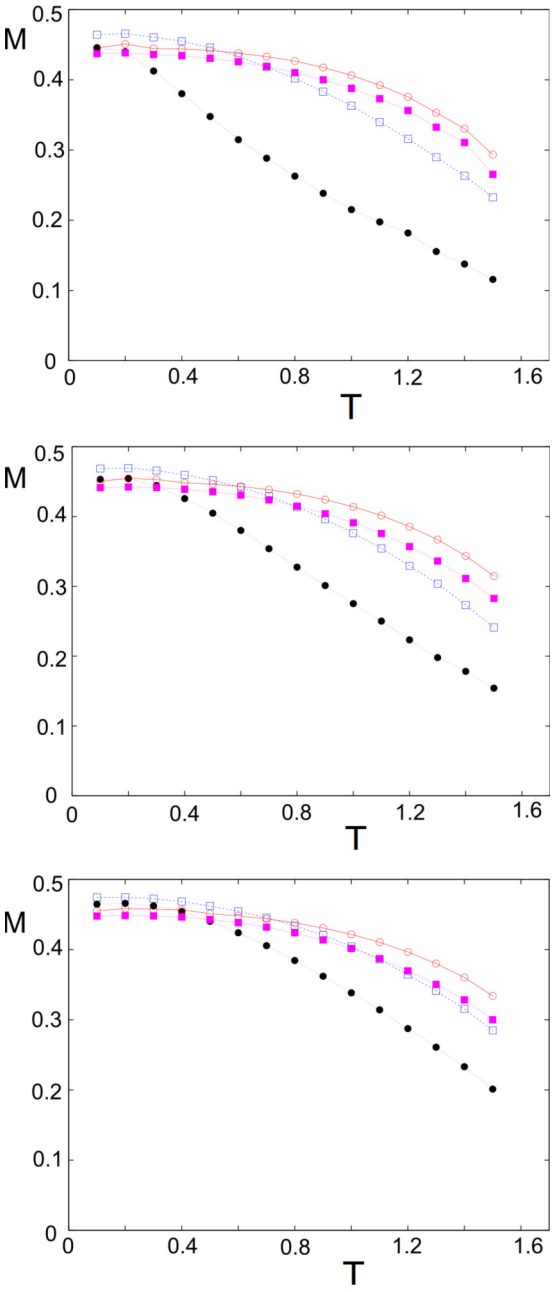

FIG. 10. (Color online) Layer magnetizations as functions of T for the surface interaction $J_1^s = 0.3$ (top), 0.5 (middle), and 0.7 (bottom) with $J_2/J_1 = -2$, $d = 0.1$, and $N_z = 16$. Black circles, blue void squares, magenta squares, and red void circles are for first, second, third, and fourth layers, respectively.

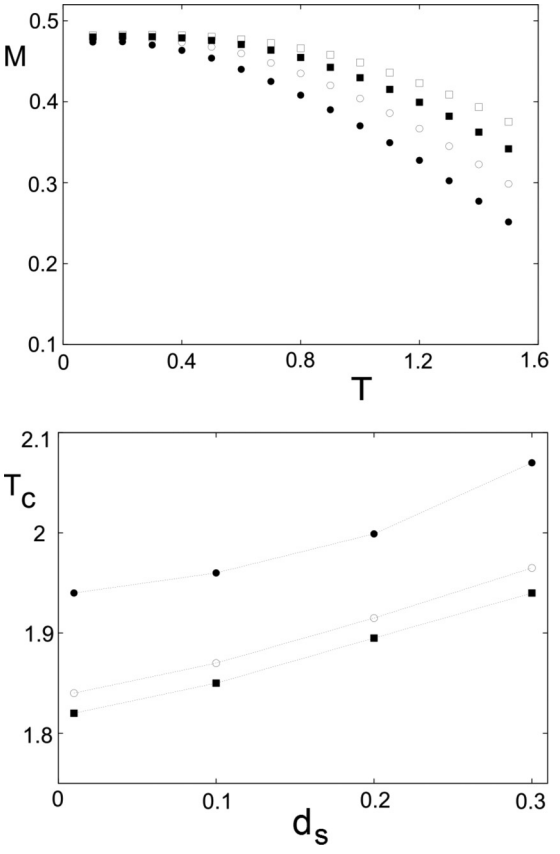

FIG. 11. Top: Surface magnetization vs T for $d_s = 0.01$ (circles), 0.1 (void circles), 0.2 (squares), and 0.3 (void squares), with $J_1^s = 1$, $J_2/J_1 = -2$, and $N_z = 16$. Bottom: Transition temperature vs d_s for $J_1^s = 0.7$, 0.5, and 0.3 (curves from up to down), with $J_2/J_1 = -2$, $d = 0.1$, and $N_z = 16$.

the bulk "rigidity" dominates the transition. This has been experimentally seen in holmium films [31].

F. Classical helimagnetic films: Monte Carlo simulation

To appreciate quantum effects causing crossovers of layer magnetizations presented above at low temperatures, we show here some results of the classical counterpart model: spins are classical XY spins of amplitude $S = 1$. We take the XY spins rather than the Heisenberg spins for comparison with the quantum case because in the latter case we have used an in-plane Ising-like anisotropy interaction d. Monte Carlo simulations have been carried out over film samples of $100 \times 100 \times 16$. Periodic boundary conditions are applied in the xy plane. We discard 1×10^6 MC steps to equilibrate the system, and another 1×10^6 MC steps are used for averaging. The layer magnetizations versus T are shown in Fig. 12 for the case where surface interaction $J_1^s = 1$ (top) and 0.3 (bottom) with $J_2/J_1 = -2$ and $N_z = 16$. One sees the following.

(i) By extrapolation there is no spin contraction at $T = 0$ and there is no crossover of layer magnetizations at low temperatures.

(ii) From the intermediate temperature region up to the transition the relative values of layer magnetizations are not always the same as in the quantum case: for example, at $T = 1.2$, one has $M_1 < M_3 < M_4 < M_2$ in Fig. 12 (top) and $M_1 < M_2 < M_4 < M_3$ in Fig. 12 (bottom), which are not the same as in the quantum case shown in Fig. 6 (top) and Fig. 10 (top).

Our conclusion is that, even at temperatures close to the transition, helimagnets may have slightly different behaviors according to their quantum or classical nature. Extensive MC simulations with size effects and detection of the order of the phase transition are not within the scope of the present paper.

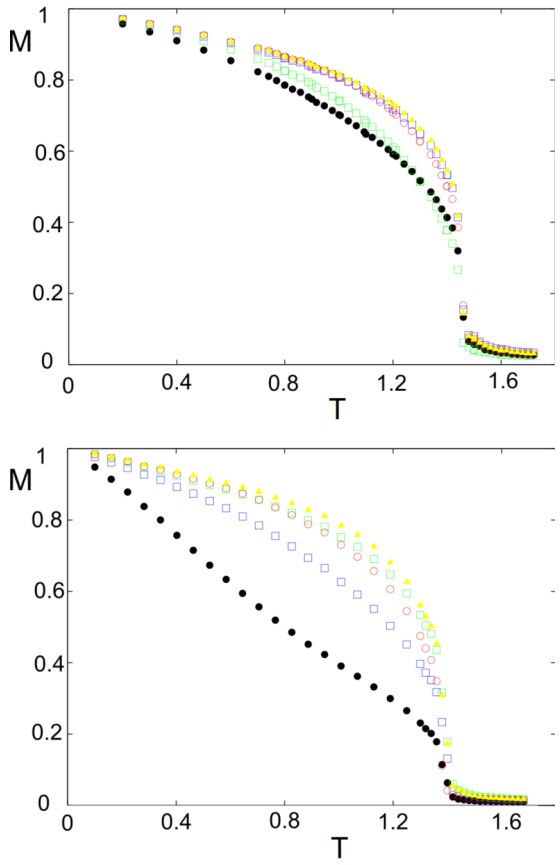

FIG. 12. (Color online) Monte Carlo results: Layer magnetizations as functions of T for the surface interaction $J_1^s = 1$ (top) and 0.3 (bottom) with $J_2/J_1 = -2$ and $N_z = 16$. Black circles, blue void squares, cyan squares, and red void circles are for first, second, third, and fourth layers, respectively.

V. CONCLUSION

We have studied in this paper surface effects in a helimagnet of a bcc lattice with quantum Heisenberg spins. Note that the method presented above can be applied to any lattice structure, and the results found in this paper are valid for general helimagnetic structures, not limited to bcc crystals. Note also that the results have been shown for the case of spin $S = 1/2$ where quantum fluctuations are strong at low temperatures. Rare-earth elements Ho and Dy with helical structures along the c axis and ferromagnetic in the basal planes which are very similar to the present model are expected to bear the same features as what has been shown above. However, at low temperatures, due to their larger spin amplitudes, $S = 7/2$ and $5/2$ for Ho and Dy, quantum fluctuations are certainly weaker, and the crossover may occur with smaller difference. Numerical applications of our formalism should be performed to get precise values for these cases.

In this paper, the classical bulk ground-state spin configuration in a thin film is exactly calculated and is found to be strongly modified near the film surface. The surface spin rearrangement is, however, limited to the first four layers in our model, regardless of the bulk angle, namely, the NNN interaction strength J_2. The spin-wave excitation is calculated using a general Green's-function technique for noncollinear spin configurations. The layer magnetization as a function of temperature as well as the transition temperature are shown for various interaction parameters. Among the striking features found in the present paper, let us mention (i) the crossover of layer magnetizations at low temperatures due to the competition between quantum fluctuations and thermal effects; (ii) the existence of low-lying surface spin-wave modes which cause a low surface magnetization; (iii) a strong effect of the surface exchange interaction (J_1^s) which drastically modifies the surface spin configuration and gives rise to a very low surface magnetization; (iv) the transition temperature, which varies strongly with the helical angle but is insensitive to the film thickness in agreement with experiments performed on MnSi films [17] and holmium [31]; and (v) the classical spin model counterpart, which gives features slightly different from those of the quantum model, both at low and high temperatures.

Let us make some comments on works of other similar models. The work by Mello *et al.* [14] has treated almost the same model as ours using a hexagonal anisotropy which corresponds to the case of Dy in which the helical angle is $\simeq 60^\circ$. However, the authors of this work studied only the classical spin configuration at $T = 0$. Unlike our work, no treatment at finite T has been considered by these authors. Rodrigues *et al.* [16] have used exactly the same model as Mello *et al.* [14] but with application to the Ho case. They have used the mean-field estimation to establish a phase diagram in the space (T, H) (H: magnetic field) and shown that surface effects affect the phase diagram. There has been, however, no detail given on surface spin configuration, surface magnetization, and quantum effects, unlike what we have done here. The MC work of Cinti *et al.* [15] was based on a classical spin model with a Hamiltonian, very different from ours, including a six-constant interaction (a kind of dipolar interaction) in the c direction.

To conclude, let us emphasize that the general theoretical method proposed here allows us to study at a microscopic level surface spin waves and their physical consequences at finite temperatures in systems with noncollinear spin configurations such as helimagnetic films. It can be used in more complicated situations such as helimagnets with Dzyaloshinskii-Moriya interactions [18].

[1] A. Yoshimori, A new type of antiferromagnetic structure in the rutile type crystal, J. Phys. Soc. Jpn. **14**, 807 (1959).

[2] J. Villain, La structure des substances magnetiques, Phys. Chem. Solids **11**, 303 (1959).

[3] I. Harada and K. Motizuki, Effect of magnon-magnon interaction on spin wave dispersion and magnon sideband in MnS, J. Phys. Soc. Jpn. **32**, 927 (1972).

[4] E. Rastelli, L. Reatto, and A. Tassi, Quantum fluctuations in helimagnets, J. Phys. C **18**, 353 (1985).

[5] H. T. Diep, Low-temperature properties of quantum Heisenberg helimagnets, Phys. Rev. B **40**, 741 (1989).

[6] R. Quartu and H. T. Diep, Phase diagram of body-centered tetragonal helimagnets, J. Magn. Magn. Mater. **182**, 38 (1998).

[7] S. M. Stishov, A. E. Petrova, S. Khasanov, G. Kh. Panova, A. A. Shikov, J. C. Lashley, D. Wu, and T. A. Lograsso, Magnetic phase transition in the itinerant helimagnet MnSi: Thermodynamic and transport properties, Phys. Rev. B **76**, 052405 (2007).

[8] H. T. Diep, Magnetic transitions in helimagnets, Phys. Rev. B **39**, 397 (1989).

[9] V. Thanh Ngo and H. T. Diep, Stacked triangular XY antiferromagnets: End of a controversial issue on the phase transition, J. Appl. Phys. **103**, 07C712 (2007).

[10] V. Thanh Ngo and H. T. Diep, Phase transition in Heisenberg stacked triangular antiferromagnets: End of a controversy, Phys. Rev. E **78**, 031119 (2008).

[11] *Frustrated Spin Systems*, edited by H. T. Diep, 2nd ed. (World Scientific, Singapore, 2013).

[12] *Ultrathin Magnetic Structures*, edited by J. A. C. Bland and B. Heinrich (Springer-Verlag, Berlin, 1994), Vols. 1 and 2.

[13] A. Zangwill, *Physics at Surfaces* (Cambridge University, Cambridge, 1988).

[14] V. D. Mello, C. V. Chianca, Ana L. Danta, and A. S. Carriç, Magnetic surface phase of thin helimagnetic films, Phys. Rev. B **67**, 012401 (2003).

[15] F. Cinti, A. Cuccoli, and A. Rettori, Exotic magnetic structures in ultrathin helimagnetic holmium films, Phys. Rev. B **78**, 020402(R) (2008).

[16] L. J. Rodrigues, V. D. Mello, D. H. A. L. Anselmo, and M. S. Vasconcelos, Magnetic structures in ultra-thin Holmium films: Influence of external magnetic field, J. Mag. Mag. Mater. **377**, 24 (2015).

[17] E. A. Karhu, S. Kahwaji, M. D. Robertson, H. Fritzsche, B. J. Kirby, C. F. Majkrzak, and T. L. Monchesky, Helical magnetic order in MnSi thin films, Phys. Rev. B **84**, 060404(R) (2011).

[18] E. A. Karhu, U. K. Rößler, A. N. Bogdanov, S. Kahwaji, B. J. Kirby, H. Fritzsche, M. D. Robertson, C. F. Majkrzak, and T. L. Monchesky, Chiral modulation and reorientation effects in MnSi thin films, Phys. Rev. B **85**, 094429 (2012).

[19] J. Heurich, J. König, and A. H. MacDonald, Persistent spin currents in helimagnets, Phys. Rev. B **68**, 064406 (2003).

[20] O. Wessely, B. Skubic, and L. Nordstrom, Spin-transfer torque in helical spin-density waves, Phys. Rev. B **79**, 104433 (2009).

[21] F. Jonietz, S. Mühlbauer, C. Pfleiderer, A. Neubauer, W. Munzer, A. Bauer, T. Adams, R. Georgii, P. Böni, R. A. Duine, K. Everschor, M. Garst, and A. Risch, Spin Transfer Torques in MnSi at Ultralow Current Densities, Science **330**, 1648 (2010).

[22] D. N. Zubarev, Double-time Green functions in statistical physics, Usp. Fiz. Nauk **71**, 71 (1960) [Sov. Phys. Usp. **3**, 320 (1960)].

[23] Diep-The-Hung, J. C. S. Levy, and O. Nagai, Effect of surface spin-waves and surface anisotropy in magnetic thin films at finite temperatures, Phys. Status Solidi B **93**, 351 (1979).

[24] V. Thanh Ngo and H. T. Diep, Effects of frustrated surface in Heisenberg thin films, Phys. Rev. B **75**, 035412 (2007); Vir. J. Nan. Sci. Tech. **15**, 126 (2007).

[25] V. Thanh Ngo and H. T. Diep, Frustration effects in antiferromagnetic face-centered cubic Heisenberg films, J. Phys: Condens. Matter **19**, 386202 (2007).

[26] E. Meloche, C. M. Pinciuc, and M. L. Plumer, Theory of surface spin waves in a stacked triangular antiferromagnet with ferromagnetic interlayer coupling, Phys. Rev. B **74**, 094424 (2006); E. Meloche, M. L. Plumer, and C. M. Pinciuc, Surface spin dynamics of antiferromagnetically coupled frustrated triangular films, *ibid.* **76**, 214402 (2007).

[27] P. Bak and M. H. Jensen, Theory of helical magnetic structures and phase transitions in MnSi and FeGe, J. Phys. C **13**, L881 (1980).

[28] M. L. Plumer and M. B. Walker, Wavevector and spin reorientation in MnSi, J. Phys. C **14**, 4689 (1981).

[29] S. V. Maleyev, Cubic magnets with Dzyaloshinskii-Moriya interaction at low temperature, Phys. Rev. B **73**, 174402 (2006).

[30] N. D. Mermin and H. Wagner, Absence of ferromagnetism or antiferromagnetism in one- or two-dimensional isotropic Heisenberg models, Phys. Rev. Lett. **17**, 1133 (1966).

[31] V. Leiner, D. Labergerie, R. Siebrecht, Ch. Sutter, and H. Zabel, Investigation of the magnetism in thin single Ho(001) films via neutron reflectivity measurements, Physica B **283**, 167 (2000).

[32] S. V. Tyablikov, Lagging and anticipating Green functions in the theory of ferromagnetism, Ukr. Mat. Zh. **11**, 289 (1959); *Methods in the Quantum Theory of Magnetism* (Plenum, New York, 1967).

[33] See, for example, H. T. Diep, *Theory of Magnetism—Application to Surface Physics* (World Scientific, Singapore, 2014).

[34] H. T. Diep, Quantum effects in antiferromagnetic thin films, Phys. Rev. B **43**, 8509 (1991).

[35] H. T. Diep, Theory of antiferromagnetic superlattices at finite temperatures, Phys. Rev. B **40**, 4818 (1989).